THE JOURNAL OF PHYSICAL CHEMISTRY C
A JOURNAL OF THE AMERICAN CHEMICAL SOCIETY

pubs.acs.org/JPCC

Article

Comparing Cyanophenyl and Pyridyl Ligands in the Formation of Porphyrin-Based Metal–Organic Coordination Networks

Brian D. Baker Cortés, Nico Schmidt, Mihaela Enache, and Meike Stöhr*

Cite This: *J. Phys. Chem. C* 2021, 125, 24557–24567

Read Online

ACCESS | Metrics & More | Article Recommendations | Supporting Information

ABSTRACT: In recent studies, porphyrin derivatives have been frequently used as building blocks for the fabrication of metal–organic coordination networks (MOCNs) on metal surfaces under ultrahigh vacuum conditions (UHV). The porphyrin core can host a variety of 3d transition metals, which are usually incorporated in solution. However, the replacement of a pre-existing metal atom in the porphyrin core by a different metallic species has been rarely reported under UHV. Herein, we studied the influence of cyanophenyl and pyridyl functional endgroups in the self-assembly of structurally different porphyrin-based MOCNs by the deposition of Fe atoms on tetracyanophenyl (Co-TCNPP) and tetrapyridyl-functionalized (Zn-TPPyP) porphyrins on Au(111) by means of scanning tunneling microscopy (STM). A comparative analysis of the influence of the cyano and pyridyl endgroups on the formation of different in-plane coordination motifs is performed. Each porphyrin derivative formed two structurally different Fe-coordinated MOCNs stabilized by three- and fourfold in-plane coordination nodes, respectively. Interestingly, the codeposited Fe atoms did not only bind to the functional endgroups but also reacted with the porphyrin core of the Zn-substituted porphyrin (Zn-TPyP), i.e., an atom exchange reaction took place in the porphyrin core where the codeposited Fe atoms replaced the Zn atoms. This was evidenced by the appearance of molecules with an enhanced (centered) STM contrast compared with the appearance of Zn-TPyP, which suggested the formation of a new molecular species, i.e., Fe-TPPyP. Furthermore, the porphyrin core of the Co-substituted porphyrin (Co-TCNPP) displayed an off-centered STM contrast after the deposition of Fe atoms, which was attributed to the binding of the Fe atoms on the top site of the Co-substituted porphyrin core. In summary, the deposition of metal atoms onto organic layers can steer the formation of structurally different MOCNs and may replace pre-existing metal atoms contained in the porphyrin core.

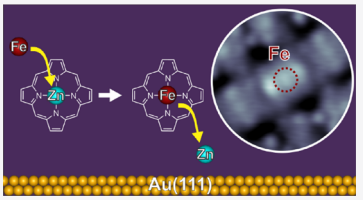

INTRODUCTION

Porphyrins are a class of macrocyclic organic molecules that play an essential role in biological processes but can be also utilized in technological applications, such as solar cells, sensors, and catalysis.[1−6] The porphyrin core, which is composed by four pyrrole moieties, can host a variety of metal atoms or remain in its free-base version.[7,8] The incorporation of the metal atom in the porphyrin core and its replacement—also known as transmetalation or atom exchange—by a different metallic species have been performed extensively in solution.[9−11] On the other hand, metalation is also possible on a surface and even under dry conditions. Several studies have reported the metalation of free-base porphyrins on noble-metal surfaces under ultrahigh vacuum (UHV) conditions as well as at the solid–liquid interface by means of the codeposition of metal atoms or coordination to substrate atoms, also known as self-metalation.[8,12−15] However, there are very few studies addressing atom exchange reactions under UHV conditions for porphyrin and porphyrin-like macrocycles, such as phthalocyanines and pyrphyrins.[16−20] In addition, most of the atom exchange studies under UHV conditions make use of X-ray absorption and photoemission spectroscopies to support their findings, and little attention has been given to the imaging capabilities of scanning tunneling microscopy (STM).[16−20] Furthermore, the porphyrin backbone can be tailored with numerous functional endgroups that grant them the possibility to form structurally different two-dimensional (2D) nanostructures that are driven by molecular self-assembly on a surface, either through directional intermolecular interactions or metal–ligand interactions in the case of metal–organic coordination networks (MOCNs).[7,8,21,22,61] In the latter case, the functional endgroups play an essential role in the formation of different in-plane coordination motifs that stabilize the structure of the MOCNs, for instance, the subtle balance between the overall shape and chemistry of the functional endgroup along with the chemical nature of the coordinating metal atoms will dictate the 2D structure of the MOCN.[7,8,21,22] In previous studies, the self-assembly of cyano-functionalized porphyrins on Au(111)[21,23,24] and Ag(111)[25−27] as well as pyridyl-functionalized porphyrins on Au(111)[5,28−32] and Ag(111)[15,27,33] has been reported.

Received: June 17, 2021
Revised: October 11, 2021
Published: October 27, 2021

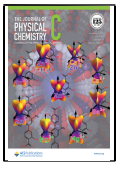

https://doi.org/10.1021/acs.jpcc.1c05360
J. Phys. Chem. C 2021, 125, 24557–24567

Herein, we present a comparative study on the deposition of Fe atoms onto self-assembled networks from cobalt(II) 5,10,15,20-(tetra-4-cyanophenyl)porphyrin (Co-TCNPP) and zinc(II) 5,10,15,20-(tetra-4-pyridyl)-21*H*,23*H*-porphyrin (Zn-TPyP) on Au(111). It was the aim to investigate whether the following processes would occur: MOCN formation, atom exchange reaction, and/or bonding of the Fe atoms on top of the porphyrin core. Comparing the influence of cyanophenyl and pyridyl ligands as well as Co and Zn contained in the porphyrin core on the above processes gives valuable additional information on the reactivities.

The chemical structures of both porphyrin derivatives are shown in Figure 1. For Co-TCNPP (Figure 1a), the

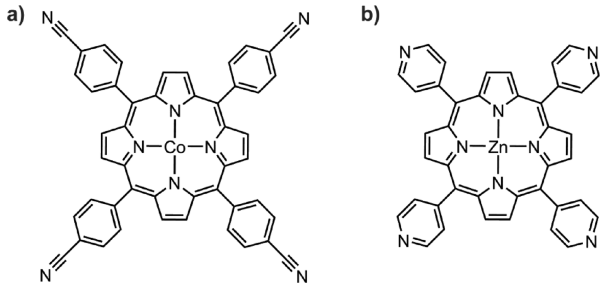

Figure 1. Chemical structures of (a) cobalt(II) 5,10,15,20-(tetra-4-cyanophenyl)porphyrin (Co-TCNPP) and (b) zinc(II) 5,10,15,20-(tetra-4-pyridyl)-21*H*,23*H*-porphyrin (Zn-TPyP).

tetrapyrrolic macrocycle is functionalized at all four meso positions by cyanophenyl endgroups, and its core contains one Co atom. On the other hand, the macrocycle of Zn-TPyP (Figure 1b) is functionalized at all four meso positions by pyridyl endgroups, and its core contains one Zn atom. As revealed by STM, the deposition of Co-TCNPP on Au(111) and subsequent deposition of Fe atoms with a fixed molecule to metal ratio (∼1:1 with a slight excess of metal) gave rise to the coexistence of two structurally different MOCNs stabilized by fourfold (grid-like network) and threefold Co-coordination nodes (chevron structure), respectively. The presence of porphyrins with a different appearance after the deposition of Fe atoms, compared with the molecular appearance shown for Co-substituted porphyrins (Co-TCNPP) in our previous work on Au(111),[21] suggested that a different molecular species was formed by two possibilities: (i) an atom exchange reaction between the Fe and Co atoms or (ii) the binding of one Fe atom on top of the porphyrin core, with the latter being the most probable possibility.[21] Furthermore, Zn-TPyP also formed two structurally different MOCNs upon coordination with Fe atoms, where threefold Fe-coordination nodes (chain-like network) were favored over the fourfold nodes (grid-like network). In contrast to the findings for Co-TCNPP, an atom exchange reaction took place where the Fe atoms replaced most of the Zn atoms in the porphyrin core of Zn-TPyP. To the best of our knowledge, we present the first detailed STM study of an atom exchange reaction under UHV conditions for long-range ordered porphyrin-based MOCNs on metal surfaces.

EXPERIMENTAL METHODS

An ultrahigh vacuum (UHV) system (with a base pressure in the low 10^{-10} mbar range) with different chambers for sample preparation and characterization was used to perform all the experiments. The Au(111) single crystal was cleaned by repeated cycles of Ar^+ sputtering and annealing at 720 K. Co-TCNPP (PorphyChem) was thermally sublimed at 820 K and Zn-TPyP (Sigma-Aldrich) at 785 K onto the Au(111) surface held at RT by means of a Knudsen cell evaporator (OmniVac). Iron atoms were deposited onto the organic layers from an iron rod using an e-beam evaporator (Oxford Applied Research) while keeping the sample at 410 K. On the other hand, for Zn-TPyP adsorbed on Au(111), iron atoms were deposited while maintaining the sample at room temperature (RT) followed by a post-annealing treatment at 440 K. The molecule−metal ratio was kept fixed (∼1:1 with a slight excess of metal) for all experiments. A quartz crystal microbalance was used to monitor the molecule and metal atom deposition rates. The STM (Scienta Omicron GmbH) measurements were performed at room temperature in the constant current mode. A mechanically cut Pt/Ir wire was used as a tip. All bias voltages were given with respect to a grounded tip. The STM images were processed with WSxM software.[34] In addition, the low-energy electron diffraction (LEED) patterns were acquired using a microchannel plate LEED (Scienta Omicron GmbH) and simulated with LEEDPat4.2 software.[35]

RESULTS

Co-TCNPP on Au(111) after Fe Deposition. As also shown in our previous study, the deposition of up to one monolayer of Co-TCNPP (Figure 1a) on Au(111) prompted the formation of a closely packed H-bonded network (see Figure S1a,b in the Supporting Information). By addition of Co atoms, the formation of both three- and fourfold MOCNs was observed independent of the initial Co-TCNPP coverage (see Figure S1c,e in the Supporting Information).[21] It should be already noted that in both assemblies, independently of the applied bias, the appearance of the porphyrin core in the STM images remained uniformly distributed among consecutive molecules since only one type of porphyrin was present, i.e., Co-TCNPP. These results serve as a reference for our present work, where the deposition of Fe atoms onto a submonolayer of Co-TCNPP molecules, while annealing the sample at 410 K and keeping a fixed molecule−metal ratio (∼1:1 with a slight excess of metal), gave rise to the coexistence of two different 2D networks as shown in Figure 2: (i) a grid-like network (Figure 2a−c and Figure S3 in the Supporting Information) and (ii) a chevron structure (Figure 2d−f).

First, we will describe the observations found for the grid-like network. In the overview STM image (Figure 2a), a densely packed array of porphyrins can be seen with molecular islands that were observed to spread over hundreds of nanometers (see Figure S3 in the Supporting Information). Individual Co-TCNPP molecules within the grid-like network can be clearly distinguished in Figure 2b. A single Co-TCNPP molecule (highlighted in yellow) appears with four bright lobes that correspond to the phenyl moieties.[25,26,36,37] The Co atom contained in the porphyrin core is not imaged at positive sample bias.[21] In addition, the herringbone reconstruction of the Au(111) surface does not translate through the molecular layer at the given imaging conditions. However, it should be noted that the herringbone reconstruction was observed on bare areas of the Au(111) surface at submonolayer coverage (see Figure S3d in the Supporting Information) entering the molecular islands and not avoiding them, which is an indication that it was preserved underneath the molecular layer.

https://doi.org/10.1021/acs.jpcc.1c05360
J. Phys. Chem. C 2021, 125, 24557−24567

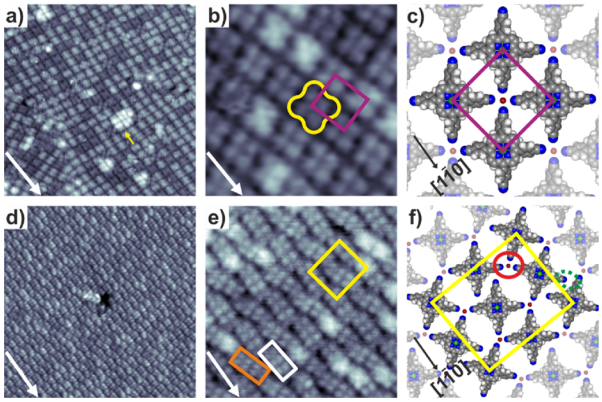

Figure 2. Self-assembly of submonolayer coverage of Co-TCNPP on Au(111) after deposition of Fe atoms: (a) STM image displaying the long-range ordered grid-like MOCN (35 × 35 nm^2, U_{bias} = −1.8 V, and I_{set} = 15 pA). The yellow arrow indicates a metallic island composed by Fe atoms. (b) High-resolution STM image of the grid-like MOCN (10 × 10 nm^2, U_{bias} = 2.2 V, and I_{set} = 15 pA). The purple square and yellow outline highlight the unit cell and one Co-TCNPP molecule, respectively. (c) Tentative structural model of the fourfold Fe-coordinated network with the unit cell depicted in purple. (d) STM image of the chevron structure (50 × 50 nm^2, U_{bias} = 2 V, and I_{set} = 15 pA). The dark region in the center of the image corresponds to missing Co-TCNPP molecules. (e) Close-up STM image of the chevron structure (18 × 18 nm^2, U_{bias} = 3 V, and I_{set} = 15 pA). The yellow rectangle highlights the unit cell, while the white and orange rectangles highlight two mirrored pairs of Co-TCNPP molecules between two rows of molecules. (f) Tentative structural model of the chevron structure with the unit cell depicted in yellow. The solid red and dotted green ovals highlight the Co-coordination and H-bonding motifs, respectively. In (c) and (f), the cobalt, iron, nitrogen, carbon, and hydrogen atoms are shown in green, red, blue, gray, and white, respectively. In (a), (b), (d), and (e), the white arrow at the bottom denotes the [1$\bar{1}$0] crystallographic direction of the Au substrate. The black arrow at the bottom in (c) and (f) denotes the [1$\bar{1}$0] crystallographic direction of the Au substrate.

From the STM and LEED measurements, a molecular overlayer (see Figure S4 in the Supporting Information) incommensurate with the Au(111) surface and having a square unit cell (shown in purple in Figure 2b,c) with lengths $a = b$ = 1.7 ± 0.1 nm and an internal angle α of 90 ± 1° was deduced. Furthermore, the unit cell is rotated 7.5° with respect to the principal Au directions (see Figure S4 in the Supporting Information). A total of one porphyrin is contained in the unit cell, giving a molecular density of 0.31 molecules per nm^2. As observed within a single unit cell, the porphyrins are pointing their cyano endgroups to a common fourfold node. Due to the repulsive interaction between electronegative N atoms from the cyano endgroups, the formation of a common fourfold node between them can be ruled out. Thus, as illustrated in the tentative structural model (Figure 2c), the grid-like network is an MOCN stabilized by metal−ligand interactions between the Fe atoms (red sphere) and porphyrins. The porphyrins form a fourfold coordination node through the terminal N atoms of the cyano endgroups and one Fe atom (Fe−N distance of ∼2.5 Å). Porphyrin-based MOCNs exhibiting fourfold coordination nodes have been previously reported for tetracyanophenyl porphyrin derivatives coordinated to Co atoms supported on a boron nitride/Cu(111) template and to Cu atoms on Cu(111).[27,37] It should be noted that the metal atoms at the coordination nodes do not contribute to the STM contrast (Figure 2), which is common for 3d transition metals in MOCNs on metallic surfaces.[38,39] Moreover, Co-TCNPP molecules rotated by 45° with respect to neighboring molecules were infrequently found in the fourfold Fe-coordinated network (see Figure S3b,c in the Supporting Information). In addition, the large bright islands observed in Figure 2a (indicated by the yellow arrow) and Figure S3d in the Supporting Information can be explained by the formation of metal clusters underneath the grid-like network from the surplus of Fe atoms.[40]

In contrast to the molecular appearance observed in the Co-coordinated fourfold MOCN (see Figure S1c−e in the Supporting Information),[21] the main observable peculiarity within the Fe-coordinated grid-like network (Figure 2a,b) is the brightness difference between consecutive molecules. The presence of bright and dim molecules at both polarities of the bias voltages—negative (Figure 2a) and positive (Figure 2b)—may be attributed to two possibilities: (i) an axial ligation of the codeposited Fe atoms with the Co atom contained in the porphyrin core and/or (ii) an atom exchange reaction between Co and Fe atoms at the porphyrin core, i.e., the deposited Fe atoms replaced some of the Co atoms that were already contained in the starting molecule (Co-TCNPP). Therefore, the grid-like network (Figure 2a,b) is composed by two different porphyrins: (i) the starting molecule (Co-TCNPP) and (ii) a molecular species formed after deposition of Fe atoms. The bright molecules in Figure 2b correspond to the newly formed porphyrin by comparing their appearance with Co-TCNPP when imaged at the same positive bias (see Figure S1c in the Supporting Information), where the Co atom inside the porphyrin core does not contribute to the STM contrast and only four bright lobes can be distinguished.[21] Our results are comparable to the findings reported for a Co-substituted tetraphenyl porphyrin on Ag(111), where the bright protrusions were attributed to Fe atoms adsorbed on top of the porphyrin core.[41] Furthermore, the studies focusing on the axial ligation of the porphyrin core under UHV conditions have been mainly performed with gaseous diatomic molecules (e.g., CO and NO),[42−47] whereas the interaction with individual atomic species has been rarely addressed.[41] In addition, atom exchange reactions in the porphyrin core are well-known in solution and have also been reported under UHV conditions for porphyrin-like molecules where the Cu-substituted molecules were replaced by Ni and Fe atoms, respectively.[12,17]

The grid-like network always coexists with a second 2D network, i.e., the chevron structure shown in Figure 2d. The molecular appearance of the porphyrins in the chevron structure (Figure 2e) is dominated by four bright lobes. Once again, the herringbone reconstruction of the Au(111) surface remained invisible underneath the 2D network. Based on the STM data, a rectangular unit cell (shown in yellow in Figure 2e,f) was obtained with dimensions a = 3.5 ± 0.2 nm and b = 4.2 ± 0.2 nm and an internal angle α of 90 ± 3°. A total of four porphyrins are contained in the unit cell, giving a molecular density of 0.27 molecules per nm^2. The porphyrins are grouped in pairs that gave rise to rows of molecules, in which the pairs from neighboring rows are mirror images of each other as highlighted by the orange and white rectangles in Figure 2e. The bonding motifs that stabilize the chevron structure are shown in the tentative structural model (Figure 2f) and will be explained by looking at a single porphyrin molecule and its surroundings. Three cyano endgroups of one porphyrin molecule coordinate to one Fe atom (solid red

https://doi.org/10.1021/acs.jpcc.1c05360
J. Phys. Chem. C 2021, 125, 24557−24567

oval), while the fourth cyano endgroup interacts via H-bonding (dotted green oval) with a H atom from the phenyl moiety of a neighboring porphyrin. By repetition of such arrangement, the chevron structure is an MOCN stabilized by a distorted threefold metal coordination (solid red oval) and H-bonding (dotted green oval). Furthermore, the distortion of the threefold coordination node arises from an asymmetrical arrangement of the porphyrins involved in metal coordination, i.e., the angle between the porphyrins involved in threefold metal coordination diverges from 120°, which is the value reported for threefold coordination motifs on metal surfaces.[48] The typical invisibility of 3d transition metals at the coordination nodes of MOCNs prevails for the chevron structure at both positive and negative bias (see Figure S5 in the Supporting Information).[38,39] Similar to the Fe-coordinated grid-like network (Figure 2a,b), the varying contrast between dim and bright molecular species is also present in the chevron structure (Figure 2d,e), which suggests the presence of Co-TCNPP and some porphyrins with an Fe atom as an axial ligand on the porphyrin core and/or substituting the initial Co atom by means of an atom exchange reaction. To gain deeper insight into this aspect, a bias-dependent experiment for the chevron structure was performed (see Figure S5 in the Supporting Information). The four bright lobe contrast is present at positive bias, and a square-like shape of the porphyrin macrocycle dominates at negative bias for Co-TCNPP. By analogy with the results obtained for Co-TCNPP with Co atoms on Au(111),[21] the porphyrin core within the Co-coordinated structure remained dim for all molecules at positive bias (see Figure S1c in the Supporting Information), which is opposite to the observed brightness difference in the chevron structure stabilized by Fe atoms (Figure 2e). The porphyrins that contain one bright protrusion (highlighted by the white arrow in Figure S5 in the Supporting Information) at all voltages can be attributed to Co-TCNPP species that contain one Fe atom as an axial ligand on top of its core (see Figure S5 in the Supporting Information). The possibility of having one Fe atom as an axial ligand on the porphyrin core and/or substituting the Co atom of the starting molecule will be addressed in the Discussion section (*vide infra*).

The chevron structure always coexists as a minority phase with the grid-like network. A 20:80 coverage ratio was found between both MOCNs for samples prepared at submonolayer coverage (~0.85 ML). It should be noted that the chevron structure did not form as one exclusive phase irrespective of the molecular coverage. In contrast, the grid-like network formed as one exclusive phase upon deposition of the required stoichiometric amount of Co-TCNPP and Fe atoms for a full monolayer of the fourfold MOCN. The 2D structure and bonding motifs of the Fe-coordinated MOCNs of Co-TCNPP are in agreement with our previous results obtained for Co-TCNPP on Au(111) upon coordination with Co atoms.[21]

Zn-TPyP on Au(111) after Fe Coordination. The deposition of submonolayer coverage of Zn-TPyP molecules (Figure 1b) on Au(111) and subsequent addition of Fe atoms followed by post-deposition annealing at 440 K and keeping a fixed molecule−metal ratio (~1:1 with a slight excess of metal) gave rise to the coexistence of two different 2D networks as shown in Figure 3: (i) a chain-like network (Figure 3a,b) and (ii) a grid-like network (Figure 3c,d). We will focus on the long-range ordered chain-like network first (see also Figure S6 in the Supporting Information). The STM image in Figure 3a shows details of the molecular appearance and orientation of

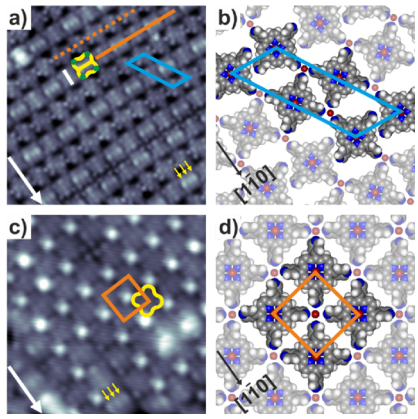

Figure 3. Self-assembly of Zn-TPyP on Au(111) after deposition of Fe atoms: (a) High-resolution STM image of the threefold Fe-coordinated chain-like network (15 × 15 nm^2, U_{bias} = −0.9 V, and I_{set} = 20 pA). The blue parallelogram depicts the oblique unit cell. The yellow and white outlines highlight two alternating Zn-TPyP molecules given by the saddle-shape conformation of the porphyrin macrocycle. The solid and dotted orange lines correspond to two different parallel rows of molecules. (b) Tentative structural model of the threefold Fe-coordinated chain-like network with the unit cell depicted in blue. (c) High-resolution STM image of the fourfold Fe-coordinated network (10 × 10 nm^2, U_{bias} = −1.6 V, and I_{set} = 15 pA). The orange square and yellow outline highlight the unit cell and one Zn-TPyP molecule, respectively. (d) Tentative structural model of the fourfold Fe-coordinated network with the unit cell depicted in orange. In (b) and (d), the iron, nitrogen, carbon, and hydrogen atoms are shown in red, blue, gray, and white, respectively. In (a) and (c), the white arrow at the bottom denotes the [1$\bar{1}$0] crystallographic direction of the Au substrate. The black arrow at the bottom in (b) and (d) denotes the [1$\bar{1}$0] crystallographic direction of the Au substrate.

the Zn-TPyP molecules within the chain-like network. At first glance, the molecules arrange in two types of parallelly oriented rows (highlighted by the solid and dotted orange lines). Within one type of row, the yellow outline highlights the rectangular shape of a single Zn-TPyP molecule with its pyridyl endgroups imaged as four small dim lobes located at the surrounding of each molecule (emphasized by the green dots in Figure 3a). The rectangular shape is given by the saddle-shape conformation adopted by Zn-TPyP upon adsorption, which creates two different side lengths by tilting upward one pair of opposing pyrrole moieties (long symmetry axis) while tilting downward the remaining pair due to steric hindrance between the H atoms of the pyrrole moieties from the porphyrin core and the pyridyl endgroups, with the latter being tilted ~60° out of the plane of the porphyrin macrocycle, as previously reported for the pyridyl endgroups of tetrapyridyl porphyrin derivatives on Ag(111) and Au(111), respectively.[28,33] This shape is representative of pyridyl-substituted porphyrins by imaging their occupied states at negative bias voltage.[28,33] Furthermore, the molecules appear to be alternately rotated by 90° with respect to their long symmetry axis (highlighted by the yellow and white lines in Figure 3a) within a single row of molecules. This arrangement of alternating molecules is given by the steric repulsion encountered between the H atoms from neighboring molecules upon adsorption on the Au(111) surface.[28,33] Based on the STM data, a unit cell (shown in blue) with lengths a = 1.4 ± 0.2 nm and b = 4.0 ± 0.1 nm and an internal angle α of 57 ± 3° was obtained. There are two Zn-

https://doi.org/10.1021/acs.jpcc.1c05360
J. Phys. Chem. C 2021, 125, 24557−24567

TPyP molecules per unit cell giving a molecular density of 0.40 molecules per nm^2.

Herein, the intermolecular interactions of the porphyrins within the two types of parallelly oriented rows (highlighted by the orange lines) will be addressed. The solid orange line highlights a row of alternating porphyrins that follow a head-to-head configuration pointing their pyridyl endgroups toward each other, similar to the molecular orientation reported for Fe-coordinated one-dimensional chains of H_2-TPyP molecules on Au(111).[29] The dotted orange line is added to distinguish the second type of molecular row, in which the alternating molecules are pointing their pyridyl endgroups toward the macrocycle of a neighboring molecule. This orientation is comparable to the one described for H_2-TPyP on Ag(111).[33] The interaction between consecutive (parallel) rows creates a common threefold node between the pyridyl endgroups from three different porphyrins. By taking electrostatic repulsion into consideration, a threefold node between the N atoms of the pyridyl endgroups without a metallic atom between them can be neglected. Therefore, as illustrated in the tentative structural model (Figure 3b), the chain-like network is an MOCN stabilized by two types of interactions: (i) a distorted threefold Fe-coordination motif between the pyridyl endgroups from three different molecules and one Fe atom (red sphere) with an Fe−N distance of ∼2.3 Å and (ii) H-bonding between the pyridyl's terminal N atom and a H atom from a neighboring pyrrole moiety (H-bonding occurs along the molecular row that is highlighted by the dotted orange line in Figure 3a).

One relevant observable feature within the chain-like network is the long bright protrusion composed by three maxima (highlighted by the three yellow arrows) along the main symmetry axis of each molecule. The STM image of the H-bonded network of Zn-TPyP on Au(111) (see Figure S2 in the Supporting Information) serves as a comparison for the contrast observed at the porphyrin core in the absence of Fe atoms and has been previously reported.[49,61] The dark spot or depression in the porphyrin core is given by the fully occupied d orbital ($3d^{10}$) of the Zn atom, which does not contribute to the STM contrast (see Figure S2 in the Supporting Information).[50] However, as shown in Figure 3a and in the bias-dependent STM images of the chain-like network (Figure 4a−d), the contrast of the three bright maxima (the white arrows mark a reference point to guide the eyes) is resilient to voltage variations (within the range of −0.9 to −2 V as mentioned in the STM data), which is an indication of an atom exchange reaction between Zn and Fe atoms in the porphyrin core. The observed brightness in the porphyrin core is well in line with previous studies of Fe-substituted tetrapyridyl and tetraphenyl porphyrin networks on Au(111) and Ag(111).[15,30,51−54] The formation of the three maxima can be explained by a combination between the saddle-shape conformation of Zn-TPyP on the Au(111) surface and the replacement of Zn atoms by Fe atoms, where the maxima located at the edges of the porphyrin core (Figure 3a) can be assigned to the two upper tilted pyrrole moieties and the central maximum is given by an Fe atom that replaced the Zn atom of Zn-TPyP. Such a molecular appearance has been reported for Fe-TPyP molecules on metal surfaces.[15,51] It should be noted that the long bright protrusion is only observed on the long symmetry axis of the molecule.

The chain-like network coexisted with a second 2D network, which will be referred to as the grid-like network (Figure 3c).

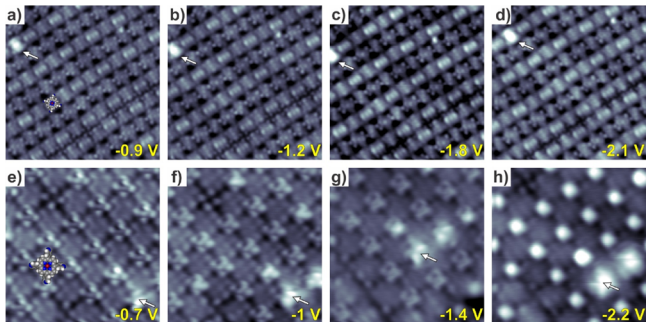

Figure 4. Bias-dependent STM images of the MOCNs formed by Zn-TPyP on Au(111) after deposition of Fe atoms: (a−d) threefold Fe-coordinated network (15 × 15 nm^2, I_{set} = 20 pA). The porphyrin core is distinguished by three protrusions attributed to a central Fe atom and two upward tilted pyrrole moieties due to the saddle-shape conformation of Zn-TPyP. (e−h) Fourfold Fe-coordinated network (7 × 7 nm^2, I_{set} = 20 pA). The appearance of the functional endgroups and iron atoms at the coordination nodes is strongly bias-dependent. The Fe-coordination nodes are observed as bright spots. The bias voltage (U_{bias}) for each STM image is indicated in yellow in the bottom right of each STM image. The white arrows serve as a guide to the eyes to one specific feature (see the text). In (a) and (e), a schematic of Zn-TPyP is added to guide the eyes, in which the iron, nitrogen, carbon, and hydrogen atoms are shown in red, blue, gray, and white, respectively.

The STM image (Figure 3c) shows tightly packed porphyrins. Similar to that in the chain-like network, a single porphyrin (highlighted in yellow) is imaged as a rectangle, and the pyridyl endgroups are imaged as small dim lobes located at the edges of each porphyrin. Once again, the saddle-shape conformation and alternating out-of-plane rotation of the pyridyl endgroups (∼60°) create two different side lengths that lead to the rectangular shape of the porphyrin macrocycle. This adsorption conformation of the porphyrin core is in line with previous reports of tetrapyridyl porphyrin assemblies on Ag(111) and Au(111), respectively.[28,33] The STM contrast observed in the porphyrin core is outweighed by the bright spots located in its periphery. These bright spots might correspond to Fe atoms, which are not typical for 3d transition metals found in MOCNs (*vide infra*). We attribute this appearance to a tip-induced effect, i.e., a functionalized tip. Furthermore, the bright contrast observed at the coordination nodes did not prevail when the sample was scanned under conventional scanning conditions, i.e., without a functionalized tip (see Figure S7 in the Supporting Information).

From the STM measurements, a unit cell (shown in orange) with lengths a = 1.4 ± 0.1 nm and b = 1.4 ± 0.2 nm and an internal angle α of 90 ± 2° was proposed. The unit cell contains one molecule giving a molecular density of 0.47 molecules per nm^2. The Zn-TPyP molecules align their pyridyl endgroups toward a common fourfold node, which suggests the presence of a metal−ligand interaction between Fe atoms (bright spots in Figure 3c) and pyridyl endgroups. We rule out the possibility of a common fourfold node between the N atoms of the pyridyl endgroups due to electrostatic repulsion. Thus, as depicted in the tentative structural model (Figure 3d), the grid-like network can be regarded as an MOCN stabilized by a fourfold Fe-coordination node formed between the terminal N atoms from four pyridyl endgroups belonging to different porphyrin molecules and one Fe atom (red sphere) acting as the coordination node with an Fe−N distance of

https://doi.org/10.1021/acs.jpcc.1c05360
J. Phys. Chem. C 2021, 125, 24557−24567

~2.2 Å. The molecular arrangement of the grid-like network is in agreement with the assembly described for pyridyl-substituted porphyrins after coordination with Fe atoms on Au(111).[5,28,29]

The set of bias-dependent STM images (Figure 4e–h) justifies the presence of the fourfold Fe-coordination motif in the grid-like network. The white arrows mark a reference point to guide the eyes. At low negative bias voltage (Figure 4e), the pyridyl endgroups are imaged as dim protrusions in the periphery of the Zn-TPyP molecules, and the Fe atoms do not contribute to the STM contrast. As the negative bias voltage approaches to higher negative values (Figure 4f–h), the contrast of the Fe atoms at the coordination nodes increases and overcomes the contribution of the pyridyl endgroups. At the highest negative bias voltage (Figure 4h), the Fe atoms appear as bright spots, and the pyridyl endgroups are barely visible. The STM contrast of the porphyrin core was not able to outweigh the contribution given by the coordinating Fe atoms, most likely because of the tip-induced effect caused during data acquisition. By taking a closer look at the porphyrin core (Figure 3c), the three maxima (highlighted by the yellow arrows) along the molecular axis are reminiscent of the appearance encountered in the chain-like network, which confirms that the atom exchange reaction between Zn and Fe atoms also holds for the grid-like network.

The grid-like network always coexists as a minority phase with the chain-like network in a 10:90 coverage ratio (for the given preparation conditions) between both MOCNs formed by Zn-TPyP molecules. Both MOCNs of Zn-TPyP were also stable at low molecular coverage (see Figures S6 and S7 in the Supporting Information). However, the grid-like network did not form as one exclusive phase. In addition, a fourfold coordination motif can be seen in the lower half of the STM image (Figure 3a) shown for the chain-like network. The presence of such a motif can be regarded as a kinetically trapped phase since annealing the Au(111) substrate at 420 K while depositing Fe atoms prompted the formation of the chain-like network as one exclusive phase.

DISCUSSION

Our discussion is aimed to explain two relevant topics in the following order: (I) a comparison of the influence of the functional endgroups from each porphyrin on the formation of different Fe-coordinated MOCNs and (II) the influence of the codeposited Fe atoms on the porphyrin core of Co-TCNPP and Zn-TPyP in view of either triggering an atom exchange reaction or the formation of an axial ligand on the porphyrin core.

(I) Fe-Coordinated MOCNs: The Influence of the Functional Endgroups. Herein, the influence of the functional endgroups (e.g., cyano and pyridyl) of each porphyrin on the formation of different bonding motifs will be addressed along with the coordination geometries of the Fe atoms stabilizing each MOCN. In 3D crystalline structures, Fe atoms prefer tetrahedral and octahedral coordination geometries.[65] However, MOCNs on surfaces were found to be stabilized by two-, three-, and fourfold in-plane Fe-coordination motifs.[5,28−32,64]

(Ia) Co-TCNPP. For the MOCNs formed by Co-TCNPP, the grid-like network (Figure 2a) was stabilized by a fourfold Fe-coordination motif and the chevron structure (Figure 2d) by a distorted threefold Fe-coordination motif as well as H-bonding. These results are structurally equivalent to the results obtained in our previous study of Co-TCNPP on Au(111) upon coordination with Co atoms (see Figure S1 in the Supporting Information).[21] However, the herringbone reconstruction of the Au(111) surface did not translate through the molecular layer of the Fe-coordinated MOCNs (Figure 2), which might suggest a stronger molecule−substrate interaction compared with our results of the Co-coordinated MOCNs of Co-TCNPP on Au(111), where the herringbone reconstruction remained visible through the 2D network after depositing Co atoms.[21] However, as previously mentioned, the herringbone reconstruction was observed on bare areas of the Au(111) surface at submonolayer coverage (see Figure S3d in the Supporting Information) entering the molecular islands and not avoiding them, which is an indication that it was preserved underneath the molecular layer. Furthermore, we propose that the Fe atoms located at the coordination nodes of the grid-like network are interacting through a square planar coordination geometry with four (in-plane) cyano endgroups.[28,29] On the other hand, the Fe atoms stabilizing the chevron structure adopted a distorted tetrahedral coordination geometry between three cyano endgroups and the Au substrate that acts as the fourth ligand. Furthermore, no substrate site-specific interactions were observed for the Fe-coordinated MOCNs of Co-TCNPP (Figure 2) as supported by the absence of integer matrix elements in the superstructure matrix of the simulated LEED pattern (see Figure S4 in the Supporting Information).[65,66]

(Ib) Zn-TPyP. For the MOCNs formed by Zn-TPyP, the chain-like network (Figure 3a) exhibited a combination of an in-plane threefold Fe-coordination motif and H-bonding. In this arrangement, the Fe atoms bonded to the pyridyl endgroups and the Au substrate follow a tetrahedral coordination geometry, as expected for Fe atoms in 3D structures. However, in-plane threefold Fe-coordination has not been reported up to now for long-range ordered MOCNs formed by tetrapyridyl porphyrins on metal surfaces, where two- and fourfold coordination motifs prevail.[5,28−30] The second MOCN of Zn-TPyP, i.e., the grid-like network of Zn-TPyP (Figure 3c), was a minority phase in which the Fe atoms arranged in an in-plane fourfold node following a square planar coordination geometry.[28,29]

By comparing the structure of the MOCNs formed by both molecules (Figure 1), they were able to form similar coordination environments (three- and fourfold motifs) with the Fe atoms through their terminal N atoms. However, as observed by the STM images (Figures 2 and 3), the structural differences between the cyanophenyl and pyridyl endgroups either allowed or obstructed the formation of higher coordination motifs within the 2D plane of the MOCN. For instance, the linear conformation of the cyano endgroups of Co-TCNPP in the grid-like network (Figure 2a) favored the formation of a higher coordination motif (e.g., fourfold Fe coordination) in the 2D plane of the MOCN compared with the threefold motif of the chain-like network of Zn-TPyP (Figure 3a). The spatial constraints that pyridyl endgroups introduce have been previously reported, where they favored two- and threefold coordination motifs.[27,67−69] For obvious reasons, the low preference of the fourfold motif encountered for Zn-TPyP (Figure 3c) was corroborated when only threefold nodes were formed by annealing the Au substrate during Fe deposition. Therefore, the grid-like network of Zn-TPyP can be considered as a kinetically trapped phase that can transform into the thermodynamically favored chain-like

https://doi.org/10.1021/acs.jpcc.1c05360
J. Phys. Chem. C 2021, 125, 24557−24567

network. As for the cyano endgroups in Co-TCNPP, their reduced steric hindrance compared with their pyridyl analogue favored the formation of fourfold nodes. This was confirmed by the formation of the grid-like network as a majority phase over the chevron structure. In summary, the cyano endgroups preferred coordinating with the Fe atoms in an in-plane fourfold geometry, whereas the pyridyl endgroups adopted a threefold node due to steric repulsion.

The aforementioned MOCNs can be compared in terms of Gibbs free energy since self-assembly is a thermodynamically driven process.[70] For Co-TCNPP, the grid-like network minimizes the surface area through its higher molecular density compared with the chevron structure and allows the formation of the square planar coordination geometry for the Fe atoms, which differs from the coordination geometry expected for Fe atoms in 3D structures.[63] In addition, the grid-like network lowers the energy of the system since only metal−ligand interactions take place in comparison with the chevron structure that possesses H-bonding along with metal−ligand interactions. Furthermore, the molecule−substrate interactions are most likely comparable for both MOCNs since no site-specific positions were observed, i.e., the MOCNs are not commensurate with the Au substrate.

In the case of Zn-TPyP (Figure 3a), the chain-like network, despite its lower molecular density and the presence of H-bonding in comparison with the grid-like network (Figure 3c), lowers the overall energy of the system by having the Fe atoms arranged in the coordination geometry expected for 3D structures (favored due to the spatial constraints of the pyridyl endgroups) and is observed as one exclusive phase upon annealing. Similar to the MOCNs of Co-TCNPP, the molecule−substrate interactions for both MOCNs of Zn-TPyP are comparable since no preferential orientation with respect to the surface was observed.

Therefore, the functional endgroups in porphyrins can steer the formation of structurally different MOCNs. In addition, the atom exchange reaction between 3d transition metals in the porphyrin core on metal surfaces is achievable under UHV, and its degree of exchange depends on the chemical nature of the metal atoms involved.

(IIa) Influence of the Codeposited Fe Atoms on the Porphyrin Core of Co-TCNPP. Since the STM contrast in metalloporphyrins is strongly mediated through the orbitals of 3d transition metals contained in the porphyrin core, the varying brightness between consecutive molecules within the MOCNs was the observable fingerprint available to determine if an atom exchange reaction or axial ligation occurred in the porphyrin core after the deposition of the Fe atoms.[15,52,53,55,56] The STM contrast observed for Co-TCNPP in the absence of Fe atoms (see Figure S1 in the Supporting Information) is in line with the reported appearance for Co-substituted porphyrins: the typical four bright lobe contrast at positive bias and the long bright protrusion along the long molecular axis (highlighted by the white dotted line in Figure S1d) at negative bias.[25,52,55,57] However, for the Fe-coordinated networks of Co-TCNPP (the grid-like network and the chevron structure in Figure 2a and Figure 2d, respectively), the increased STM contrast stemming from the core of some molecules, in comparison with the appearance of Co-TCNPP with codeposited Co atoms (see Figure S1 in the Supporting Information), suggested a modification in the porphyrin core induced by the codeposited Fe atoms either as an (i) axial ligand on the core or (ii) by the atom exchange reaction.

We will first address the possibility of an axial ligation on top of the porphyrin core. The position of the bright centers in the porphyrin core of both networks (the grid-like network and the chevron structure in Figure 2b and Figure 2e, respectively) is off-centered and remained unaffected even when imaged at positive bias. In order to gain further insight, we performed bias-dependent imaging (ranging from positive to negative bias) for the chevron structure (see Figure S5 in the Supporting Information). The molecules with an enhanced STM contrast (one marked by the white arrow in Figure S5) remained bright irrespective of the bias polarity. As previously reported, the porphyrin core of Fe-substituted porphyrins on metal substrates contributes to the STM contrast depending on the value of the applied bias.[15,47] In addition, the bright STM contrast independent of the applied bias does not convey the overall emblem that is characteristic of Fe-substituted porphyrins when imaged at negative bias, i.e., three maxima along the long molecular axis of the porphyrin backbone or a dumbbell-like appearance depending on the applies bias.[15,51,52] On the other hand, the appearance of the other (dim) molecules was modified with the applied bias and even displayed the typical four bright lobe contrast when imaged at positive bias (see Figure S5a,b in the Supporting Information), which is in line with the appearance of Co-TCNPP molecules. The enhanced STM contrast of the molecules displaying an off-centered (see Figure S3h in the Supporting Information) brightness with respect to the porphyrin core can be explained by the bonding of one Fe atom as an axial ligand on top of the porphyrin core. Therefore, the increased height of the Fe atoms with respect to the molecular plane of the 2D MOCNs confers them a brighter STM contrast than its surroundings, i.e., the Fe atom bonded on top of the porphyrin core sits higher than any other adsorbate on the Au(111) surface. These findings are well in line with a previous report of the adsorption of Fe atoms as axial ligands on the porphyrin core of Co-substituted tetraphenyl porphyrins on Ag(111).[41] In this study, the Fe atoms were not adsorbed centered and occupied one of the four equivalent positions of the porphyrin core, for which each equivalent position is composed by the hexamer formed by two neighboring pyrrole moieties of the porphyrin core, i.e., the Co−N−C−C−C−N cyclic subunit.[41] Within our study, we attribute a similar adsorption geometry to the codeposited Fe atoms (observed in Figure 2b,e). In addition, the height profiles (see Figure S3e−f in the Supporting Information) of bare Co-TCNPP and Fe on top of Co-TCNPP are ∼2 and 4.2 Å, respectively, and are in line with the previously reported values of Fe atoms sitting on top of Co-substituted tetraphenyl porphyrins on Ag(111).[41]

Based on these arguments, an atom exchange reaction between the codeposited Fe atoms and Co atoms in Co-TCNPP seems unlikely. However, we do not fully rule out this possibility since some of these molecules do not resemble the off-centered brightness, which was attributed to the axial ligation of Fe atoms bonded on top of the porphyrin core. Instead, they display a very bright protrusion along their long symmetry axis after Fe deposition (as observed in Figure 2a and Figure S3a,g in the Supporting Information), which is in line with the previously reported appearance of Fe-substituted porphyrins when imaged at negative bias.[15,51,52] The difference in the STM contrast between Co-TCNPP and the (possibly) Fe-substituted porphyrins can be explained by the population of the d orbital of the Co and Fe atoms contained in the porphyrin core, respectively. The Co atom has a $3d^7$ electronic

https://doi.org/10.1021/acs.jpcc.1c05360
J. Phys. Chem. C 2021, 125, 24557−24567

configuration with its energy levels distributed far enough from each other that allows them to be resolved by changing the polarity of the applied bias (see Figure S1 in the Supporting Information).[52,58] In contrast, the Fe atom has a $3d^6$ electronic configuration with its energy levels too close to each other, which makes it complicated to resolve different energy levels in Fe-substituted porphyrins within the same polarity of the applied bias, i.e., for Fe-substituted porphyrins, a four bright lobe contrast prevails at positive bias, while a long bright protrusion is observed at negative bias.[15,52,59]

Despite the fact that enough Fe atoms were added to cover or replace all the Co atoms contained in the Co-TCNPP molecules deposited on the Au(111) surface, the yield of brighter molecules after Fe deposition was around one-third as revealed by the STM images (Figure 2). Although the detailed mechanisms of an axial ligation or an atom exchange reaction in the porphyrin core are beyond the scope of this publication and the capabilities of a typical STM measurement, we assume that a similar value of binding energies for the Co and Fe atoms can explain why most of the Fe atoms bonded to the porphyrin core in an off-centered configuration on top of the porphyrin core instead of replacing the Co atoms.[60] In summary, most of the bright molecules possess an Fe atom bonded on top of their core, while some molecules might have experienced an atom exchange reaction where the Co atom of the starting molecules was replaced by one of the codeposited Fe atoms.

(IIb) Influence of the Codeposited Fe Atoms on the Porphyrin Core of Zn-TPyP. A slightly different scenario was observed for both MOCNs of Zn-TPyP (Figure 3) in comparison with the MOCNS of Co-TCNPP. As previously mentioned, the long bright protrusion composed by three maxima along the main symmetry axis of the porphyrin correlates to the fingerprint observed for Fe-substituted porphyrins functionalized with pyridyl endgroups when imaged at negative bias.[15,51,52] This molecular appearance was present for all the porphyrins in the chain-like and grid-like networks and differs completely from the dark depression observed for Zn-substituted porphyrins (see Figure S2 in the Supporting Information).[48,49,60] The fully occupied d orbital ($3d^{10}$) of Zn atoms in combination with the larger calculated HOMO−LUMO gap for Zn-substituted porphyrins compared to Fe-substituted porphyrins (*vide supra*) explains their dark appearance under STM.[59] The atom exchange reaction between Zn and Fe atoms was fully efficient as revealed by the STM images (Figure 3 and Figure S6 in the Supporting Information) and correlates to the lower binding energy toward the porphyrin core found for Zn atoms with respect to Fe atoms.[60] Therefore, the energy barrier that an Fe atom must overcome to replace a Zn atom must be lower than the barrier to replace the Co atom and agrees with the universal stability order found for metal porphyrins, where metals with an increased occupation of the d orbital, such as Zn atoms, have lower stability within the porphyrin core.[17,60,62]

CONCLUSIONS

In the present study, the influence of the deposition of Fe atoms on the self-assembly of two porphyrin derivatives (Co-TCNPP and Zn-TPyP) was investigated by STM under UHV conditions. Special attention was given to the possibility of 2D MOCN formation, an atom exchange reaction in the porphyrin core and bonding of the Fe atoms on top of the porphyrin core. Upon deposition of Fe atoms, each porphyrin gave rise to the coexistence of two structurally different Fe-coordinated MOCNs stabilized by three- or fourfold Fe-coordination nodes. However, the structural differences between both functional endgroups (cyano and pyridyl endgroups in Co-TCNPP and Zn-TPyP, respectively) strictly determined the formation of a specific in-plane coordination motif. As evidenced by STM, the linear conformation of the cyano endgroups (Co-TCNPP) allowed the formation of a higher in-plane coordination motif as the majority phase, i.e., fourfold Fe coordination (grid-like network) over threefold Fe coordination (chevron structure). In contrast, the steric hindrance that pyridyl endgroups (Zn-TPyP) encounter in higher coordination motifs favored the formation of threefold Fe-coordination nodes (chain-like network) over fourfold Fe coordination (fourfold coordinated network). In the case of Co-TCNPP, the grid-like network reduced the overall energy of the system, i.e., by densely packing the molecules (reducing the surface area covered by Co-TCNPP) and forming metal−ligand interactions only, the grid-like network was favored over the chevron structure. In the case of Zn-TPyP, the higher surface area of the chain-like network was compensated by the reduction of steric hindrance between neighboring pyridyl endgroups and by having the Fe atoms in a tetrahedral coordination geometry, which is the coordination geometry expected for Fe atoms in 3D structures.

In addition, within each MOCN, the presence of molecules with a brighter STM contrast in each MOCN, compared with their 2D assemblies prior to Fe deposition, served as the fingerprint to determine if the Fe atoms interacted with the porphyrin core either by (i) bonding as an axial ligand on the core or (ii) replacing the pre-existing metal atom via an atom exchange reaction. The yield of brighter molecules was lower for Co-TCNPP (∼1/3 of the molecules on the surface) than for Zn-TPyP (∼100%). However, the molecular appearance of the bright Co-TCNPP molecules differed from that of the bright Zn-TPyP molecules, i.e., an off-centered brightness in some Co-TCNPP molecules suggested that the Fe atoms did not replace the Co atom but instead bonded on top of the porphyrin core. On the other hand, the bright Zn-TPyP molecules resembled the molecular appearance of Fe-TPyP, meaning that the Fe atoms replaced the Zn atoms via an atom exchange reaction. This behavior was explained by the lower binding energy that Zn atoms possess toward the porphyrin core in comparison with Co atoms. On the other hand, despite that Fe and Co atoms possess similar binding energies toward the porphyrin core, the Fe atoms were not able to replace the Co atoms and instead bonded on top of the porphyrin core. In summary, the choice of the functional endgroups in metalloporphyrins will strongly influence the coordination geometry for the metal atoms stabilizing the MOCN. In addition, atom exchange reactions are achievable under UHV, and their yield is dependent on, among others, the chemical nature of the metal atoms involved, i.e., their binding energy toward the porphyrin core. In the present study, both metal−ligand interactions and atom exchange reactions were observed. Further studies are required to address which of these reactions takes place first.

ASSOCIATED CONTENT

Supporting Information

The Supporting Information is available free of charge at https://pubs.acs.org/doi/10.1021/acs.jpcc.1c05360.

https://doi.org/10.1021/acs.jpcc.1c05360
J. Phys. Chem. C 2021, 125, 24557−24567

Additional STM data given for Co-TCNPP coordinated to Co atoms on Au(111), Co-TCNPP coordinated to Fe atoms on Au(111), Zn-TPyP on Au(111), and Zn-TPyP coordinated to Fe atoms on Au(111); LEED pattern of the fourfold Fe-coordinated network formed by Co-TCNPP on Au(111) after the deposition of Fe atoms (PDF)

AUTHOR INFORMATION

Corresponding Author

Meike Stöhr − *Zernike Institute for Advanced Materials, University of Groningen, 9747 AG Groningen, The Netherlands*; orcid.org/0000-0002-1478-6118; Email: m.a.stohr@rug.nl

Authors

Brian D. Baker Cortés − *Zernike Institute for Advanced Materials, University of Groningen, 9747 AG Groningen, The Netherlands*

Nico Schmidt − *Zernike Institute for Advanced Materials, University of Groningen, 9747 AG Groningen, The Netherlands*

Mihaela Enache − *Zernike Institute for Advanced Materials, University of Groningen, 9747 AG Groningen, The Netherlands*

Complete contact information is available at: https://pubs.acs.org/10.1021/acs.jpcc.1c05360

Notes

The authors declare no competing financial interest.

ACKNOWLEDGMENTS

This work was supported by the Netherlands Organization for Scientific Research (NWO) (Vici grant 680.47.633) and by the Zernike Institute for Advanced Materials of the University of Groningen.

REFERENCES

(1) Oohora, K.; Hayashi, T. Hemoprotein-Based Supramolecular Assembling Systems. *Curr. Opin. Chem. Biol.* **2014**, *19*, 154−161.

(2) Chae, S. H.; Yoo, K.; Lee, Y. S.; Cho, M. J.; Kim, J. H.; Ko, M. J.; Lee, S. J.; Choi, D. H. Novel π-Extended Porphyrin Derivatives for Use in Dye-Sensitized Solar Cells. *J. Porphyrins Phthalocyanines* **2014**, *18*, 569−578.

(3) Hadmojo, W. T.; Lee, U.-H.; Yim, D.; Kim, H. W.; Jang, W.-D.; Yoon, S. C.; Jung, I. H.; Jang, S.-Y. High-Performance Near-Infrared Absorbing n-Type Porphyrin Acceptor for Organic Solar Cells. *ACS Appl. Mater. Interfaces* **2018**, *10*, 41344−41349.

(4) Lvova, L.; Mastroianni, M.; Pomarico, G.; Santonico, M.; Pennazza, G.; Di Natale, C.; Paolesse, R.; D'Amico, A. Carbon Nanotubes Modified with Porphyrin Units for Gaseous Phase Chemical Sensing. *Sens. Actuators, B.* **2012**, *170*, 163−171.

(5) Wurster, B.; Grumelli, D.; Hötger, D.; Gutzler, R.; Kern, K. Driving the Oxygen Evolution Reaction by Nonlinear Cooperativity in Bimetallic Coordination Catalysts. *J. Am. Chem. Soc.* **2016**, *138*, 3623−3626.

(6) Tempas, C. D.; Morris, T. W.; Wisman, D. L.; Le, D.; Din, N. U.; Williams, C. G.; Wang, M.; Polezhaev, A. V.; Rahman, T. S.; Caulton, G.; et al. Redox-Active Ligand Controlled Selectivity of Vanadium Oxidation on Au(100). *Chem. Sci.* **2018**, *9*, 1674−1685.

(7) Auwärter, W.; Écija, D.; Klappenberger, F.; Barth, J. V. Porphyrins at Interfaces. *Nat. Chem.* **2015**, *7*, 105−120.

(8) Gottfried, J. M. Surface Chemistry of Porphyrins and Phthalocyanines. *Surf. Sci. Rep.* **2015**, *70*, 259−379.

(9) Lavallee, D. K. Kinetics and Mechanisms of Metalloporphyrin Reactions. *Coord. Chem. Rev.* **1985**, *61*, 55−96.

(10) Hambright, P.; Batinić-Haberle, I.; Spasojević, I. Meso tetrakis ortho-, meta-, and para-N-alkylpyridiniopor-Phyrins: Kinetics of Copper(II) and Zinc(II) Incorporation and Zinc Porphyrin Demetalation. *J. Porphyrins Phthalocyanines* **2003**, *07*, 139−146.

(11) Buchler, J. W. *Porphyrins and Metalloporphyrins*; Smith, K. M., Ed.; Elsevier: Asmterdam, 1975.

(12) Diller, K.; Papageorgiou, A. C.; Klappenberger, F.; Allegretti, F.; Barth, J. V.; Auwärter, W. In Vacuo Interfacial Tetrapyrrole Metallation. *Chem. Soc. Rev.* **2016**, *45*, 1629−1656.

(13) Marbach, H. Surface-Mediated *in Situ* Metalation of Porphyrins at the Solid−Vacuum Interface. *Acc. Chem. Res.* **2015**, *48*, 2649−2658.

(14) Gottfried, J. M.; Flechtner, K.; Kretschmann, A.; Lukasczyk, T.; Steinrück, H.-P. Direct Synthesis of a Metalloporphyrin Complex on a Surface. *J. Am. Chem. Soc.* **2006**, *128*, 5644−5645.

(15) Auwärter, W.; Weber-Bargioni, A.; Brink, S.; Riemann, A.; Schiffrin, A.; Ruben, M.; Barth, J. V. Controlled Metalation of Self-Assembled Porphyrin Nanoarrays in Two Dimensions. *ChemPhysChem* **2007**, *8*, 250−254.

(16) Doyle. Ni−Cu Ion Exchange Observed for Ni(II)-porphyrins on Cu(111). *Chem. Commun.* **2014**, *50*, 3447−3449, DOI: 10.1039/c3cc48913b.

(17) Rieger, A.; Schnidrig, S.; Probst, B.; Ernst, K. H.; Wäckerlin, C. Ranking the Stability of Transition-Metal Complexes by On-Surface Atom Exchange. *J. Phys. Chem. Lett.* **2017**, *8*, 6193−6198.

(18) Shen, K.; Narsu, B.; Ji, G.; Sun, H.; Hu, J.; Liang, Z.; Gao, X.; Li, H.; Li, Z.; Song, B.; et al. On-Surface Manipulation of Atom Substitution Between Cobalt Phthalocyanine and the Cu(111) Substrate. *RSC Adv.* **2017**, *7*, 13827−13835.

(19) Hötger, D.; Abufager, P.; Morchutt, C.; Alexa, P.; Grumelli, D.; Dreiser, J.; Stepanow, S.; Gambardella, P.; Busnengo, H. F.; Etzkorn, M.; Gutzler, R.; Kern, K. On-Surface Transmetalation of Metalloporphyrins. *Nanoscale* **2018**, *10*, 21116−21122.

(20) Herritsch, J.; Kachel, S. R.; Fan, Q.; Hutter, M.; Heuplick, L. J.; Münster, F.; Gottfried, J. M. On-Surface Porphyrin Transmetalation with Pb/Cu Redox Exchange. *Nanoscale* **2021**, *13*, 13241−13248.

(21) Baker Cortés, B. D.; Schmidt, N.; Enache, M.; Stöhr, M. Coverage-Dependent Structural Transformation of Cyano-Functionalized Porphyrin Networks on Au(111) via Addition of Cobalt Atoms. *J. Phys. Chem. C* **2019**, *123*, 19681−19687.

(22) Baker Cortés, B. D.; Stöhr, M. Role of Cyano Groups in the Self-Assembly of Organic Molecules on Metal Surfaces. In *Encyclopedia of Interfacial Chemistry*; Wandelt, K., Ed.; Elsevier, 2018; Vol. *4*, pp. 153−165, DOI: 10.1016/B978-0-12-409547-2.13540-1.

(23) Yokoyama, T.; Yokoyama, S.; Kamikado, T.; Okuno, Y.; Mashiko, S. Selective Assembly on a Surface of Supramolecular Aggregates with Controlled Size and Shape. *Nature* **2001**, *413*, 619−621.

(24) Pham, T. A.; Song, F.; Alberti, M. N.; Nguyen, M.-T.; Trapp, N.; Thilgen, C.; Diederich, F.; Stöhr, M. Heat-Induced Formation of One-Dimensional Coordination Polymers on Au(111): An STM Study. *Chem. Commun.* **2015**, *51*, 14473−14476.

(25) Lepper, M.; Schmitt, T.; Gurrath, M.; Raschmann, M.; Zhang, L.; Stark, M.; Hölzel, H.; Jux, N.; Meyer, B.; Schneider, M. A.; et al. Adsorption Behavior of a Cyano-Functionalized Porphyrin on Cu(111) and Ag(111): From Molecular Wires to Ordered Supramolecular Two-Dimensional Aggregates. *J. Phys. Chem. C* **2017**, *121*, 26361−26371.

(26) Urgel, J. I.; Ecija, D.; Auwärter, W.; Stassen, D.; Bonifazi, D.; Barth, J. V. Orthogonal Insertion of Lanthanide and Transition-Metal Atoms in Metal−Organic Networks on Surfaces. *Angew. Chem. Int. Ed.* **2015**, *127*, 6261−6265.

(27) Bischoff, F.; He, Y.; Seufert, K.; Stassen, D.; Bonifazi, D.; Barth, J. V.; Auwärter, W. Tailoring Large Pores of Porphyrin Networks on Ag(111) by Metal−Organic Coordination. *Chem. − Eur. J.* **2016**, *22*, 15298−15306.

(28) Wang, Y.; Zhou, K.; Shi, Z.; Ma, Y.-q. Structural Reconstruction and Spontaneous Formation of Fe Polynuclears: A Self-Assembly of Fe−Porphyrin Coordination Chains on Au(111) Revealed by Scanning Tunneling Microscopy. *Phys. Chem. Chem. Phys.* **2016**, *18*, 14273−14278.
(29) Lin, T.; Kuang, G.; Wang, W.; Lin, N. Two-Dimensional Lattice of Out-of-Plane Dinuclear Iron Centers Exhibiting Kondo Resonance. *ACS Nano* **2014**, *8*, 8310−8316.
(30) Liu, B.; Fu, H.; Guan, J.; Shao, B.; Meng, S.; Guo, J.; Wang, W. An Iron-Porphyrin Complex with Large Easy-Axis Magnetic Anisotropy on Metal Substrate. *ACS Nano* **2017**, *11*, 11402−11408.
(31) Shi, Z.; Lin, N. Structural and Chemical Control in Assembly of Multicomponent Metal−Organic Coordination Networks on a Surface. *J. Am. Chem. Soc.* **2010**, *132*, 10756−10761.
(32) Mao, X. F.; Lin, T.; Adisoejoso, J.; Shi, Z.; Shang, X. S.; Liu, P. N.; Lin, N. Coordination Self-Assembly of Bromo-Phenyl and Pyridyl Functionalized Porphyrins with Fe on an Au(111) Surface. *Phys. Chem. Chem. Phys.* **2013**, *15*, 12447−12450.
(33) Auwärter, W.; Weber-Bargioni, A.; Riemann, A.; Schiffrin, A.; Gröning, O.; Fasel, R.; Barth, J. V. Self-Assembly and Conformation of Tetrapyridyl-Porphyrin Molecules on Ag(111). *J. Chem. Phys.* **2006**, *124*, 194708−194708/6.
(34) Horcas, I.; Fernández, R.; Gómez-Rodríguez, J. M.; Colchero, J.; Gómez-Herrero, J.; Baro, A. M. Wsxm: A Software for Scanning Probe Microscopy and a Tool for Nanotechnology. *Rev. Sci. Instrum* **2007**, *78*, No. 013705.
(35) Hermann, K.; van Hove, M. A. *LEEDpat4.2 (LEED pattern analyzer)*; Fritz Haber Institute: 2015. http://www.fhi-berlin.mpg.de/KHsoftware/LEEDpat/index.html (accessed Sep 21, 2018).
(36) Auwärter, W.; Seufert, K.; Klappenberger, F.; Reichert, J.; Weber-Bargioni, A.; Verdini, A.; Cvetko, D.; Dell'Angela, M.; Floreano, L.; Cossaro, A.; et al. Site-Specific Electronic and Geometric Interface Structure of Co-Tetraphenyl-Porphyrin Layers on Ag(111). *Phys. Rev. B* **2010**, *81*, 245403/1−245403/14.
(37) Urgel, J. I.; Schwarz, M.; Garnica, M.; Stassen, D.; Bonifazi, D.; Ecija, D.; Barth, J. V.; Auwärter, W. Controlling Coordination Reactions and Assembly on a Cu(111) Supported Boron Nitride Monolayer. *J. Am. Chem. Soc.* **2015**, *137*, 2420−2423.
(38) Björk, J.; Matena, M.; Dyer, M. S.; Enache, M.; Lobo-checa, J.; Gade, L. H.; Jung, T. A.; Stöhr, M.; Persson, M. STM Fingerprint of Molecule−Adatom Interactions in a Self-Assembled Metal−Organic Surface Coordination Network on Cu(111). *Phys. Chem. Chem. Phys.* **2010**, *12*, 8815−8821.
(39) Henningsen, N.; Rurali, R.; Limbach, C.; Drost, R.; Pascual, J. I.; Franke, K. J. Site-Dependent Coordination Bonding in Self-Assembled Metal−Organic Networks. *J. Phys. Chem. Lett.* **2011**, *2*, 55−61.
(40) Buchner, F.; Kellner, I.; Steinrück, H.-P.; Marbach, H. Modification of the Growth of Iron on Ag(111) by Predeposited Organic Monolayers. *Z. Phys. Chem.* **2009**, *223*, 131−144.
(41) Vijayaraghavan, S.; Auwärter, W.; Ecija, D.; Seufert, D.; Rusponi, S.; Houwaart, T.; Sautet, P.; Bocquet, M.-L.; Thakur, P.; Stepanow, S.; Schlickum, U.; Etzkorn, M.; Brune, H.; Barth, J. V. Restoring the Co Magnetic Moments at Interfacial Co-Porphyrin Arrays by Site-Selective Uptake of Iron. *ACS Nano* **2015**, *9*, 3605−3616.
(42) Seufert, K.; Auwärter, W.; Barth, J. V. Discriminative Response of Surface-Confined Metalloporphyrin Molecules to Carbon and Nitrogen Monoxide. *J. Am. Chem. Soc.* **2010**, *132*, 18141−18146.
(43) Wäckerlin, C.; Chylarecka, D.; Kleibert, A.; Müller, K.; Lacovita, C.; Nolting, F.; Jung, T. A.; Ballav, N. Controlling Spins in Adsorbed Molecules by a Chemical Switch. *Nat. Commun.* **2010**, *1*, 61.
(44) Hieringer, W.; Flechtner, K.; Kretschmann, A.; Seufert, K.; Auwärter, W.; Barth, J. V.; Görling, A.; Steinrück, H.-P.; Gottfried, J. M. The Surface Trans Effect: Influence of Axial Ligands on the Surface Chemical Bonds of Adsorbed Metalloporphyrins. *J. Am. Chem. Soc.* **2011**, *133*, 6206−6222.
(45) Miguel, J.; Hermanns, C. F.; Bernien, M.; Krüger, A.; Kuch, W. Reversible Manipulation of the Magnetic Coupling of Single Molecular Spins in Fe-Porphyrins to a Ferromagnetic Substrate. *J. Phys. Chem. Lett.* **2011**, *2*, 1455−1459.
(46) Kim, H.; Chang, Y. H.; Lee, S.-H.; Kim, Y.-H.; Kahng, S.-J. Switching and Sensing Spin States of Co-Porphyrin in Bimolecular Reactions on Au(111) Using Scanning Tunneling Microscopy. *ACS Nano* **2013**, *7*, 9312−9317.
(47) Wäckerlin, C.; Nowakowski, J.; Liu, S.-X.; Jaggi, M.; Siewert, D.; Girovsky, J.; Shchyrba, A.; Hählen, T.; Kleibert, A.; Oppeneer, P. M.; et al. Two-Dimensional Supramolecular Electron Spin Arrays. *Adv. Mater.* **2013**, *25*, 2404−2408.
(48) Schlickum, U.; Decker, R.; Klappenberger, F.; Zoppellaro, G.; Klyatskaya, S.; Ruben, M.; Silanes, I.; Arnau, A.; Kern, K.; Brune, H.; et al. Metal−Organic Honeycomb Nanomeshes with Tunable Cavity Size. *Nano Lett.* **2007**, *7*, 3813−3817.
(49) Shi, Z.; Lin, N. Self-Assembly of a Two-Dimensional Bimetallic Coordination Framework and Dynamic Control of Reversible Conversions to Homo-Metallic Hydrogen-Bond Arrays. *ChemPhysChem* **2010**, *11*, 97−100.
(50) Yoshimoto, S.; Tsutsumi, E.; Suto, K.; Honda, Y.; Itaya, K. Molecular Assemblies and Redox Reactions of Zinc (II) Tetraphenylporphyrin and Zinc (II) Phthalocyanine on Au(111) Single Crystal Surface at Electrochemical Interface. *Chem. Phys.* **2005**, *319*, 147−158.
(51) Zotti, L. A.; Teobaldi, G.; Hofer, W. A.; Auwa, W.; Barth, J. V. Ab-Initio Calculations and STM Observations on Tetrapyridyl and Fe(II)-Tetrapyridyl-Porphyrin Molecules on Ag(111). *Surf. Sci.* **2007**, *601*, 2409−2414.
(52) Buchner, F.; Warnick, K.-G.; Wölfle, T.; Görling, A.; Steinrück, H.-P.; Hieringer, W.; Marbach, H. Chemical Fingerprints of Large Organic Molecules in Scanning Tunneling Microscopy: Imaging Adsorbate−Substrate Coupling of Metalloporphyrins. *J. Phys. Chem. C* **2009**, 16450−16457.
(53) Wang, W.; Pang, R.; Kuang, G.; Shi, X.; Shang, X.; Liu, P. N.; Lin, N. Intramolecularly Resolved Kondo Resonance of High-Spin Fe(II)-Porphyrin Adsorbed on Au(111). *Phys. Rev. B: Condens. Matter Mater. Phys.* **2015**, *91*, No. 045440.
(54) Buchner, F.; Schwald, V.; Comanici, K.; Steinrück, H.-P.; Marbach, H. Microscopic Evidence of the Metalation of a Free-Base Porphyrin Monolayer with Iron. *ChemPhysChem* **2007**, *8*, 241−243.
(55) Houwaart, T.; Le Bahers, T.; Sautet, P.; Auwärter, W.; Seufert, K.; Barth, J. V.; Bocquet, M.-L. Scrutinizing Individual CoTPP Molecule Adsorbed on Coinage Metal Surfaces from the Interplay of STM Experiment and Theory. *Surf. Sci.* **2015**, *635*, 108−114.
(56) Comanici, K.; Buchner, F.; Flechtner, K.; Lukasczyk, T.; Gottfried, J. M.; Steinrück, H. P.; Marbach, H. Understanding the Contrast Mechanism in Scanning Tunneling Microscopy (STM) Images of an Intermixed Tetraphenylporphyrin Layer on Ag(111). *Langmuir* **2008**, *24*, 1897−1901.
(57) Brede, J.; Linares, M.; Kuck, S.; Schwöbel, J.; Scarfato, A.; Chang, S. H.; Hoffmann, G.; Wiesendanger, R.; Lensen, R.; Kouwer, P. H. J.; Hoogboom, J.; Rowan, A. E.; Bröring, M.; Funk, M.; Stafström, S.; Zerbetto, F.; Lazzaroni, R. Dynamics of Molecular Self-Ordering in Tetraphenyl Porphyrin Monolayers on Metallic Substrates. *Nanotechnology* **2009**, *20*, 275602.
(58) Lu, X.; Hipps, K. W.; Wang, X. D.; Mazur, U. Scanning Tunneling Microscopy of Metal Phthalocyanines: d^7 and d^9 Cases. *J. Am. Chem. Soc.* **1996**, *118*, 7197−7202.
(59) Lu, X.; Hipps, K. W. Scanning Tunneling Microscopy of Metal Phthalocyanines: d^6 and d^8 Cases. *J. Phys. Chem. B* **1997**, *101*, 5391−5396.
(60) Liao, M.-S.; Scheiner, S. Electronic Structure and Bonding in Metal Porphyrins, Metal=Fe, Co, Ni, Cu. *J. Chem. Phys.* **2002**, *117*, 205−219.
(61) Ruggieri, C.; Rangan, S.; Bartynski, R. A.; Galoppini, E. Zinc(II) Tetraphenylporphyrin Adsorption on Au(111): An Interplay between Molecular Self-Assembly and Surface Stress. *J. Phys. Chem. C* **2015**, *119*, 6101−6110.

(62) Feixas, F.; Solà, M.; Swart, M. Chemical Bonding and Aromaticity In Metalloporphyrins. *Can. J. Chem.* **2009**, *87*, 1063−1073.
(63) Venkataraman, D.; Du, Y.; Wilson, S. R.; Hirsch, K. A.; Zhang, P.; Moore, J. S. A Coordination Geometry Table of the d-Block Elements and Their Ions. *J. Chem. Educ.* **1997**, *8*, 915−918.
(64) Shi, Z.; Liu, J.; Lin, T.; Xia, F.; Liu, P. N.; Lin, N. Thermodynamics and Selectivity of Two-Dimensional Metallo-Supramolecular Self-Assembly Resolved at Molecular Scale. *J. Am. Chem. Soc.* **2011**, *133*, 6150−6153.
(65) Buchner, F.; Zillner, E.; Röckert, M.; Gläßel, S.; Steinrück, H.-P.; Marbach, H. Substrate-Mediated Phase Separation of Two Porphyrin Derivatives on Cu(111). *Chem. − Eur. J.* **2011**, *17*, 10226−10229.
(66) Yanagi, H.; Mukai, H.; Ikuta, K.; Shibutani, T.; Kamikado, T.; Yokoyama, S.; Mashiko, S. Molecularly Resolved Dynamics for Two-Dimensional Nucleation of Supramolecular Assembly. *Nano Lett.* **2002**, *2*, 601−604.
(67) Li, Y.; Xiao, J.; Shubina, T. E.; Chen, M.; Shi, Z.; Schmid, M.; Steinrück, H.-P.; Gottfried, J. M.; Lin, N. Coordination and Metalation Bifunctionality of Cu with 5,10,15,20-Tetra(4- Pyridyl)-Porphyrin: Toward a Mixed-Valence Two-Dimensional Coordination Network. *J. Am. Chem. Soc.* **2012**, *134*, 6401−6408.
(68) Heim, D.; Seufert, K.; Auwärter, W.; Aurisicchio, C.; Fabbro, C.; Bonifazi, D.; Barth, J. V. Surface-Assisted Assembly of Discrete Porphyrin-Based Cyclic Supramolecules. *Nano Lett.* **2010**, *10*, 122−128.
(69) Heim, D.; Écija, D.; Seufert, K.; Auwärter, W.; Aurisicchio, C.; Fabbro, C.; Bonifazi, D.; Barth, J. V. Self-Assembly of Flexible One-Dimensional Coordination Polymers on Metal Surfaces. *J. Am. Chem. Soc.* **2010**, *132*, 6783−6790.
(70) Enache, M.; Maggini, L.; Llanes-Pallas, A.; Jung, T. A.; Bonifazi, D.; Stöhr, M. Coverage-Dependent Disorder-to-Order Phase Transformation of a Uracil Derivative on Ag(111). *J. Phys. Chem. C* **2014**, *118*, 15286−15291.

https://doi.org/10.1021/acs.jpcc.1c05360
J. Phys. Chem. C 2021, 125, 24557−24567